A phase-space formulation for elastic-wave traveltime tomography

Eric Chung[1], Jianliang Qian[2], Gunther Uhlmann[3], Hong-Kai Zhao[4]

[1]Applied and Computational Mathematics, California Institute of Technology, Pasadena, CA 91125, USA.
[2]Department of Mathematics, Michigan State University, East Lansing, MI 48824, USA.
[3]Department of Mathematics, University of Washington, Seattle, WA 98195, USA.
[4]Department of Mathematics, University of California, Irvine, CA 92697-3875, USA.

E-mail: tschung@acm.caltech.edu, qian@math.msu.edu, gunther@math.washington.edu, zhao@math.uci.edu

Abstract. We adopt a recent work in Chung, Qian, Uhlmann and Zhao (Inverse Problems, 23(2007) 309-329) to develop a phase space method for reconstructing pressure wave speed and shear wave speed of an elastic medium from travel time measurements. The method is based on the so-called Stefanov-Uhlmann identity which links two Riemannian metrics with their travel time information. We design a numerical algorithm to solve the resulting inverse problem. The algorithm is a hybrid approach that combines both Lagrangian and Eulerian formulations. In particular the Lagrangian formulation in phase space can take into account multiple arrival times naturally, while the Eulerian formulation for wave speeds allows us to compute the solution in physical space. Numerical examples are shown to validate the method.

1. Introduction

We address numerically the inverse problem of determining pressure (P) wave speed and shear (S) wave speed in elastic solids from P-wave and S-wave traveltime information. Different from acoustic media in which there is only one propagation mode, elastic solids accommodate more than one propagation mode. In 3-D isotropic elastic media, we have one P-wave and two S-waves [1]; in 3-D anisotropic elastic media, we have one quasi-P wave and two quasi-S waves [20, 24, 25, 23]. To reconstruct P-wave and S-wave speeds in elastic media from traveltime information in one unified framework, we adopt our recent work [5] to this new setting, assuming that in smooth elastic media P-wave and S-wave traveltimes can be identified and separated in traveltime data obtained in the application of transmission tomography [21].

All the traditional methods of travel-time tomography are directly based on Fermat's least travel-time principle and bear a close link to the X-ray computerized tomography (CT) used in medical diagnosis. In medical CT the measured data are assumed to be modeled by line integrals of wave amplitude attenuation for straight ray-paths passing through the body, and the Radon transform provides the foundation for medical CT. However, in seismics the ray-path curvature has to be taken into account in that lithology and structure usually have strong inhomogeneity, and the resulting ray-paths can depend strongly on the unknown wave speeds. To achieve such a purpose, ray-tracing based travel-time tomography methods require very complicated data structure to trace curved rays through each pixel [3]; see [35] for 3-D examples. In addition,

such ray-tracing based methods inevitably produce irregular ray coverage of the computational domain, and the resulting system of equations may not be well-conditioned.

The problem of determining the Riemannian metric from first arrivals is known in differential geometry as the boundary rigidity problem. The travel time information is encoded in the boundary distance function, which measures the distance, with respect to the Riemannian metric, between boundary points; see [31] and references therein for more information.

On the other hand, since multi-valued travel-times and resulting multipathings are common in complex velocity structures, it is necessary to take into account all the arrivals systematically. To use all arrivals in transmission tomography in an Eulerian framework, the works in [13, 11] formulated transmission tomography by using the Liouville equation based PDE framework in phase space.

The problem of determining the index of refraction from multiple arrival times is called in differential geometry as the lens rigidity problem [32]. The information is encoded in the scattering relation which gives the exit point and direction of a geodesic if we know the incoming point and direction plus also the travel time.

Our approach is based on the Stefanov-Uhlmann identity in phase space [30], and the identity was first developed into a numerical method for traveltime tomography in [5], which enables us to take into account multiple arrivals systematically and treat caustics naturally. See [13] for a related phase space formulation based on Liouville equations.

The advantages of phase space formulation are multi-fold. As a first advantage multipathing can be taken into account systematically, as evidenced in [13, 5] and references therein. As demonstrated in [8, 14], multipathing is essential for high resolution seismic imaging. As a second advantage, our phase space formulation has the potential to recover generic (anisotropic) Riemannian metrics, and also parameters of anisotropic elastic solids (see Remarks 2-4). These advantages distinguish our new method from other traditional methods in inverse kinematic problems [3, 26, 27, 28, 4, 35, 12] in that those traditional methods only recover isotropic metrics by using first-arrivals. Moreover, our numerical algorithm is based on a hybrid approach. A Lagrangian formulation (ray tracing) is used in phase space for the linearized Stefanov-Uhlmann identity. This allows us to deal with multipathing naturally. On the other hand, a Eulerian formulation is used for pressure wave speed or shear wave speed of an elastic medium. As a consequence our computational domain is in physical space rather than in phase space.

The paper is organized as follows. Section 2 provides the necessary background for elastic wave traveltime tomography. In Section 3, we state the inverse problem, linearize the Stefanov-Uhlmann identity, and propose a nonlinear functional as the foundation for solving the inverse problem in phase space. In Section 4, we show examples to demonstrate the effectiveness of the phase space method. Section 5 concludes the paper.

2. Background

In elastic solids there are more than one propagation mode for elastic waves. In isotropic media we have pressure (P) waves and shear (S) waves, and in anisotropic media we also have more than one type of shear waves.

In an isotropic-elastic solid without body force, the displacement vector $\mathbf{u}$ satisfies [9]

$$\nabla \cdot \big(\mu(\nabla \mathbf{u} + \nabla \mathbf{u}^T)\big) + \nabla(\lambda \nabla \cdot \mathbf{u}) = \rho \ddot{\mathbf{u}} \tag{1}$$

where λ and μ are Lame's elastic parameters, and ρ is the density.

When the elastic body is homogeneous, the displacement vector $\mathbf{u}$ satisfies a simplified linear elastic wave equation,

$$\mu \nabla^2 \mathbf{u} + (\lambda + \mu) \nabla \nabla \cdot \mathbf{u} = \rho \ddot{\mathbf{u}} \tag{2}$$

where λ and μ are constants.

Representing $\mathbf{u}$ in equation (2) in terms of the scalar potential ψ^p and the vector potential ψ^s,

$$\mathbf{u} = \nabla\psi^p + \nabla \times \psi^s, \tag{3}$$

the above equation of motion decouples into two wave equations for the potential [21]

$$\nabla^2\psi^p = \frac{1}{v_p^2}\ddot{\psi}^p, \tag{4}$$

$$\nabla^2\psi^s = \frac{1}{v_s^2}\ddot{\psi}^s, \tag{5}$$

where

$$v_p^2 = \frac{\lambda + 2\mu}{\rho} \quad \text{and} \quad v_s^2 = \frac{\mu}{\rho}. \tag{6}$$

In the high frequency regime, we seek solutions in the asymptotic form

$$\psi^p(x,t) = A^p(x,t)f(t - \phi_p(x)), \tag{7}$$

$$\psi^s(x,t) = A^s(x,t)f(t - \phi_s(x)), \tag{8}$$

where f is some waveform function, A^p and A^s are amplitudes. Then we have two eikonal equations for P-wave traveltime function, ϕ_p, and S-wave traveltime function, ϕ_s, respectively,

$$\|\nabla\phi_p(x)\|^2 = \frac{1}{v_p^2}, \tag{9}$$

$$\|\nabla\phi_s(x)\|^2 = \frac{1}{v_s^2}. \tag{10}$$

We remark that one can also directly insert the following ansatz into the equation (1)

$$\mathbf{u} = \mathbf{A}(x,t)f(t - \phi(x))$$

to obtain the eikonal equations for P and S waves [1, 20]. By considering the leading-order singularity corresponding to f'', which yields eikonal equations for different waves, we realize that the terms corresponding to f'' result from the second order derivatives of u only. Furthermore, the resulting eikonal equations have the same form as equations (9) and (10), where now v_p and v_s are varying functions of spatial position x. Consequently, without loss of generality we will model P-wave and S-wave traveltimes by equations (9) and (10) with varying speed functions v_p or v_s, respectively.

To carry out transmission traveltime tomography, we assume that in smooth elastic media P-wave and S-wave traveltimes can be identified and separated in traveltime data obtained in the application of transmission tomography [21]. This assumption enables us to adopt the framework in [5] to reconstruct P-wave and S-wave speeds from their traveltimes satisfying the eikonal equations (9), (10).

3. Methodology

The framework developed in [5] is valid for reconstructing a general Riemannian metric in a bounded domain by a set of boundary measurements. In the following we outline the basic setup and specify the formulation to the setting of an elastic medium.

3.1. Basic setup

Let $\Omega \subset \mathbb{R}^n$ be a bounded domain with smooth boundary $\Gamma = \partial\Omega$. Let $g(x) = (g_{ij}(x))$ be a Riemannian metric in Ω. Let $d_g(x, y)$ denote the geodesic distance between x and y. The inverse problem is whether we can determine the Riemannian metric g up to the natural obstruction of a diffeomorphism by knowing $d_g(x, y)$ for any $x \in \Gamma$ and $y \in \Gamma$.

While theoretically there are a lot of works addressing this question (see [18, 19, 17, 2, 29, 6, 22] and references therein), following the successful work in [5] we explore the possibility to recover isotropic metrics in elastic media numerically. We use a phase space formulation so that multipathing in physical space is allowed. Rather than the boundary distance function we look at the *scattering relation* which measures the point and direction of exit of a geodesic plus the travel time if we know the point and direction of entrance of the geodesic. Such data are available in practice; see [5, 13] and references therein. Below we formulate more precisely the problem.

Assume that we have two C^k metrics g_1 and g_2 with $k \geq 2$ satisfying $g_1 = g_2$ in $\mathbb{R}^n - \Omega$.

The Hamiltonian H_g related to g is

$$H_g(x, \xi) = \frac{1}{2}(\Sigma_{i,j=1}^n g^{ij}(x)\xi_i\xi_j - 1), \tag{11}$$

where g is either g_1 or g_2, and $g^{-1} = (g^{ij})$.

Let $X := (x, \xi)$. We denote by $X_{g_j}(s, X^{(0)}) = (x_{g_j}(s, X^{(0)}), \xi_{g_j}(s, X^{(0)}))$, $j = 1, 2$, the solution to the Hamiltonian system defined by $H_{g_j}(x, \xi) = 0$,

$$\frac{dx}{ds} = \frac{\partial H_{g_j}}{\partial \xi}, \quad \frac{d\xi}{ds} = -\frac{\partial H_{g_j}}{\partial x}, \tag{12}$$

with the initial condition $X^{(0)} = (x^0, \xi^0)$, where $x^0 \in \mathbb{R}^n$ and $\xi^0 \in S_g^{n-1}(x^0)$. Here we define the unit sphere in the cotangent space $T_x^*(\mathbb{R}^n)$:

$$S_g^{n-1}(x) := \left\{ \xi \in T_x^*(\mathbb{R}^n) : H_g(x, \xi) = \frac{1}{2}(\Sigma_{i,j=1}^n g^{ij}(x)\xi_i\xi_j - 1) = 0 \right\}. \tag{13}$$

The continuous dependence on the initial data of the solution of the Hamiltonian system is characterized by the Jacobian,

$$J_{g_j}(s) = J_{g_j}\left(s, X^{(0)}\right) := \frac{\partial X_{g_j}}{\partial X^{(0)}}\left(s, X^{(0)}\right). \tag{14}$$

It can be shown easily from the definition of J and the corresponding Hamiltonian system (12) [7] that J_{g_j}, $j = 1, 2$, satisfies

$$\frac{dJ}{ds} = M\ J, \quad J(0) = I, \tag{15}$$

where, in terms of $H = H_{g_j}$ $(j = 1, 2)$, the matrix M is defined by

$$M = \begin{pmatrix} H_{\xi,x}, & H_{\xi,\xi} \\ -H_{x,x}, & -H_{x,\xi} \end{pmatrix}. \tag{16}$$

Since $H_{g_j} \in C^k(T^*(\mathbb{R}^n))$ $(j = 1, 2)$, where $T^*(\mathbb{R}^n)$ denotes the cotangent bundle on Ω, according to the standard theory $X_{g_j} \in C^{k-1}$ jointly in $s \in \mathbb{R}$ and $X^{(0)} \in \{(x^0, \xi^0) : x^0 \in \mathbb{R}^n, \quad \xi^0 \in S_g^{n-1}(x^0)\}$ ([33], page 30.)

3.2. Linearizing the Stefanov-Uhlmann identity

Given boundary measurements for g_1, we are interested in recovering the metric g_1.

Take $X^{(0)} = (x^0, \xi^0)$, where $x^0 \in \Gamma$ and $\xi^0 \in S_g^{n-1}(x^0)$, such that the inflow condition holds,

$$\nu(x^0) \cdot g^{-1}\xi^0 < 0, \tag{17}$$

where $\nu(x^0)$ is the outer normal to $\Gamma = \partial\Omega$ at x^0, and g is either g_1 or g_2. In general, we let $\mathcal{S}^-$ and $\mathcal{S}^+$ be subsets of $\mathbb{R}^{2n}$ defined by

$$\begin{aligned} \mathcal{S}^- &= \{(x,\xi) \mid x \in \Gamma, \xi \in S_g^{n-1}(x), g^{-1}\xi \cdot \nu(x) < 0\}, \\ \mathcal{S}^+ &= \{(x,\xi) \mid x \in \Gamma, \xi \in S_g^{n-1}(x), g^{-1}\xi \cdot \nu(x) > 0\}, \end{aligned}$$

where $\nu(x)$ is the outward normal vector at $x \in \Gamma$; they correspond to the inflow and outflow conditions in phase space.

We link two metrics by introducing the function

$$F(s) := X_{g_2}(t - s, X_{g_1}(s, X^{(0)})),$$

where $t = \max(t_{g_1}, t_{g_2})$ and $t_g = t_g(X^{(0)})$ is the length of the geodesic issued from $X^{(0)}$ with the endpoint on Γ. Consequently, we have the following Stefanov-Uhlmann identity [30]

$$\begin{aligned} &X_{g_1}(t, X^{(0)}) - X_{g_2}(t, X^{(0)}) \\ &= \int_0^t \frac{\partial X_{g_2}}{\partial X^{(0)}} \left(t - s, X_{g_1}(s, X^{(0)})\right) \times \left(V_{g_1} - V_{g_2}\right)\left(X_{g_1}(s, X^{(0)})\right) ds, \end{aligned} \tag{18}$$

where

$$V_{g_j} := \left(\frac{\partial H_{g_j}}{\partial \xi}, -\frac{\partial H_{g_j}}{\partial x}\right) = \left(g^{-1}\xi, -\frac{1}{2}\nabla_x (g^{-1}\xi) \cdot \xi\right). \tag{19}$$

Linearizing the right hand side in the above identity, we have the following formula,

$$\begin{aligned} &X_{g_1}(t, X^{(0)}) - X_{g_2}(t, X^{(0)}) \\ &= \int_0^t J_{g_2} \left(t - s, X_{g_2}(s, X^{(0)})\right) \times \partial_{g_2} V_{g_2}(g_1 - g_2)(X_{g_2}(s, X^{(0)})) \, ds, \end{aligned} \tag{20}$$

where $\partial_g V_g(\lambda)$ is the derivative of V_g with respect to g at λ. This is the foundation for our numerical procedure.

A few remarks are in order here.

Remark 1. In the case of the isotropic metric, we have

$$(g_k)_{ij} = \frac{1}{c_k^2}\delta_{ij}, \tag{21}$$

which links directly to an eikonal equation of the same form as in equations (9) and (10). Then

$$V_{g_k} = (c_k^2 \xi, -(\nabla c_k) c_k |\xi|^2). \tag{22}$$

Hence the derivative of V with respect to g, $\partial_g V_g(\lambda)$ in the equation (20), is given by

$$\partial_g V_g(\lambda) = (2c\lambda\xi, -(\nabla c \cdot \lambda + \nabla\lambda \cdot c)|\xi|^2), \tag{23}$$

since phase space variable ξ is fixed along the given path $X_{g_2}(s, X^{(0)})$.

Remark 2. Our approach can be applied to an elastodynamical system with residual stress as

well [10]. In this case we have two Riemannian metrics with extra terms associated with the residual stress tensor [10]; they correspond to compressional waves and shear waves, respectively. Accordingly, we are able to identify and separate traveltimes of shear waves from those of compressional waves in boundary measurements [10].

Remark 3. In fact, the Stefanov-Uhlmann identity holds for any Hamiltonian in phase space rather than just Riemannian-metric-induced Hamiltonians; consequently, our approach works in a more general setting. For instance, in anisotropic elastic solids we have one quasi-P wave mode and two quasi-S wave modes; the Hamiltonian corresponding to quasi-P waves is induced by a Finsler metric rather than a Riemannian metric; see [24, 25, 23] for such examples of quasi-P Hamiltonians.

Remark 4. Since, in general, quasi-P waves are faster than quasi-S waves [20, 24, 25, 23], we can assume that corresponding traveltimes can be identified and separated from those of other waves. Therefore, it is possible to apply our approach to anisotropic elastic solids as well.

3.3. Continuous Tikhonov regularization

Given boundary measurements $X_{g_1}(t, X^{(0)}) \in \mathcal{S}^+$, where $X^{(0)} \in \mathcal{S}^-$, we recover g_1 by Newton's method via the linearization (20). During each iteration, we solve the first kind integral equation (20) by a regularization method.

For a given metric g_2 we define a linear operator, the X-ray transform via the Hamiltonian flow X_{g_2}, to map a function $\tilde{g} \in C_0^k(\mathbb{R}^n)$ into the set of its line integrals:

$$\begin{aligned} &K : \tilde{g} \in C_0^k(\mathbb{R}^n) \to K\tilde{g} \in C^k(\mathcal{S}^-), \\ &K\tilde{g} = \int_0^{t_{g_2}(\cdot)} J_{g_2}\left(t_{g_2}(\cdot) - s, X_{g_2}(s,\cdot)\right) \times \partial_{g_2} V_{g_2}(\tilde{g})\left(X_{g_2}(s,\cdot)\right)\, ds, \end{aligned}$$

$$\begin{aligned} K\tilde{g}(X^{(0)}) \;&=\; \int_0^{t_{g_2}(X^{(0)})} J_{g_2}\left(t_{g_2}(X^{(0)}) - s, X_{g_2}(s, X^{(0)})\right) \times \partial_{g_2} V_{g_2}(\tilde{g})\left(X_{g_2}(s, X^{(0)})\right)\, ds, \\ &\text{for } X^{(0)} \in \mathcal{S}^-. \end{aligned} \tag{24}$$

We define the data element as

$$\tilde{d} = X_{g_1}(t,\cdot) - X_{g_2}(t,\cdot), \tag{25}$$

where $\tilde{d} \in C^k(\mathcal{S}^-)$. Hence we have a first kind operator equation by equation (20),

$$K\tilde{g} = \tilde{d}. \tag{26}$$

By the method of regularization we introduce a nonzero parameter β and a functional,

$$G_\beta(\tilde{g}) = \frac{1}{2}\|K\tilde{g} - \tilde{d}\|^2_{\mathcal{L}^2(\mathcal{S}^-)} + \frac{1}{2}\beta\|\nabla\tilde{g}\|^2_{\mathcal{L}^2(\Omega)}, \tag{27}$$

which is defined on the domain of the gradient operator ∇. Then we seek an element $\tilde{g}_\beta$ solving the minimizing problem,

$$G_\beta(\tilde{g}_\beta) = \inf_{\tilde{g} \in D(\nabla)} G_\beta(\tilde{g}), \tag{28}$$

where $D(\nabla)$ is the domain of ∇. Under appropriate conditions we may show that the $\tilde{g}_\beta$ converges to a least squares solution $\tilde{g}_0$ of equation (26) [15, 16].

In general Newton's method for the nonlinear equation (18) based on solving the linearized problem (20) iteratively may not converge for an arbitrary initial guess. However, since stability and uniqueness are proved for a metric close to the isotropic metric [30, 34], this enables us to develop a continuation (homotopy) method. A series of intermediate metrics can be created continuously from an appropriately known metric, such as an isotropic metric, to the unknown metric by interpolation of the data. See [5] for more details.

3.4. Numerical discretization

We use a hybrid approach to solve this problem numerically. The metric g is defined on an Eulerian grid. The linearized integral equation (20) is treated in phase space using a Lagrangian formulation. Hence multipathing can be dealt with easily. The main task in the numerical computation is the discretization of the linearized integral equation (20). Since the integral is defined along the ray in a given metric, we first solve the ray equation (12) in phase space starting from a particular $X_j^{(0)}$. At the same time we compute the Jacobian matrix along the ray according to (15). Standard ODE solvers are used to solve these ODEs. On the ray, values of g are computed by interpolation from the neighboring grid point values. Hence each integral equation along a particular ray yields a linear equation for grid values of g near the ray path in the physical domain. We form a whole system of linear equations using all rays corresponding to the given measurements. This system may be under or over determined and may not have a unique solution. We regularize the system as in the continuous case discussed in Section 3.3. See [5] for more details.

4. Numerical examples

In the numerical examples, we are mainly interested in v_p and v_s. However, we notice that once we have v_p and v_s, we can reconstruct the Lame elastic parameters right away according to equation (6).

In the numerical examples, the measurement is generated by solving Hamiltonian systems for eikonal equations with true speed functions v_p and v_s, respectively. The initial data for Hamiltonian systems are chosen so that each initial data point $X^{(0)}$ contains two components $x^{(0)}$ and $\xi^{(0)}$, which are the initial physical location and the initial momentum variable, respectively; in turn, the initial momentum variable determines the corresponding initial ray direction according to the Hamiltonian system.

We take $\Omega = [0,1] \times [0,1]$ and use a regular $(N+1) \times (N+1)$ grid to discretize this domain. We put a source at every boundary grid point except those located at the corner. That is, there are totally $4(N-1)$ sources on the boundary, and at each source we initiate a number of rays with different initial ray directions.

4.1. Model 1

We assume that

$$v_p = 3, \quad v_s = 2 \quad \text{and} \quad \rho = 2.5.$$

The initial guesses are

$$v_p^{(0)} = 1 \quad \text{and} \quad v_s^{(0)} = 1$$

and the regularization parameter $\beta = 10^{-10}$. We use $N = 10$ and shoot 10 rays at each source on the boundary. The algorithm recovers both v_p and v_s exactly using 8 iterations and 9 iterations, respectively. In Figure 1 and Figure 2, we plot the successive errors for the numerical solutions. We see that the algorithm converges at the 7-th iteration.

In Figure 3 and Figure 4, we also plot the residual errors for the numerical solutions. We see that the numerical solutions are already very accurate after 5 iterations.

4.2. Model 2

We assume that

$$v_p = 3 - e^{-2((x-0.5)^2+(y-0.5)^2)}, \quad v_s = 1 + 0.2\sin(\pi x)\sin(0.5\pi y) \quad \text{and} \quad \rho = 2.5.$$

The initial guesses are

$$v_p^{(0)} = 1.5 \quad \text{and} \quad v_s^{(0)} = 1.15,$$

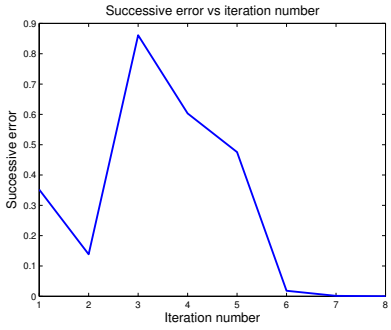

Figure 1. Model 1: Successive error vs iteration number for v_p.

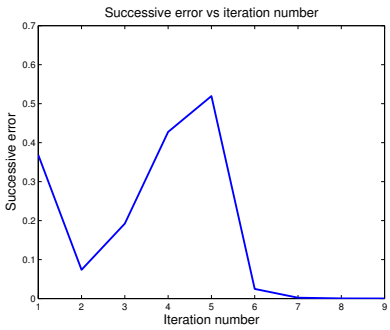

Figure 2. Model 1: Successive error vs iteration number for v_s.

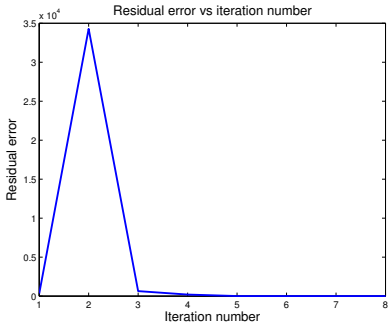

Figure 3. Model 1: Residual error vs iteration number for v_p.

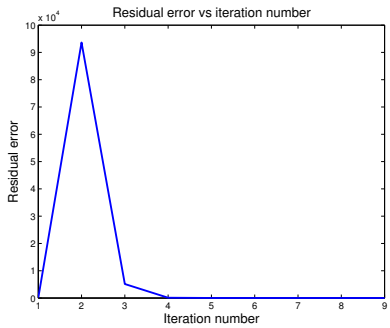

Figure 4. Model 1: Residual error vs iteration number for v_s.

and the regularization parameter $\beta = 10^{-6}$. We use $N = 16$ and shoot 20 rays at each source on the boundary. The algorithm stops when the successive error is less than 2×10^{-5}. In Figure 5 and Figure 6, we plot the successive errors for the numerical solutions. We see that the numerical results for the P-wave speed, v_p, and the S-wave speed, v_s, converge after 10 and 14 iterations, respectively.

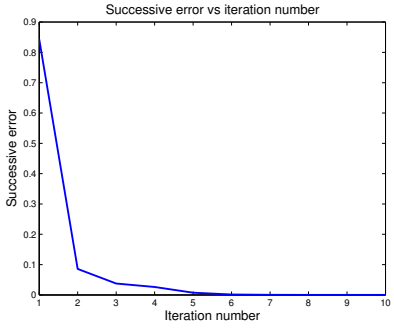

Figure 5. Model 2: Successive error vs iteration number for v_p.

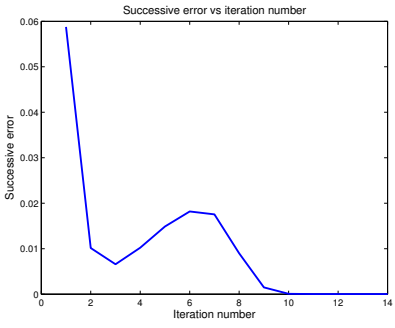

Figure 6. Model 2: Successive error vs iteration number for v_s.

As for relative numerical errors of the P-wave speed, the relative error initially is 0.3519, and the relative error at the 10-th iteration is 0.0023; thus the relative error is reduced by 153 times

in 10 iterations. Similar behavior is observed for relative errors of the S-wave speed.

In Figure 7, we compare the numerical solution for v_p at the 10th iteration with the exact solution for v_p at $x = 0.5$. In Figure 8, we compare the numerical solution for v_s at the 14-th iteration with the exact solution for v_p at $x = 0.5$. As we can see, the reconstruction results approximate the exact solutions very well.

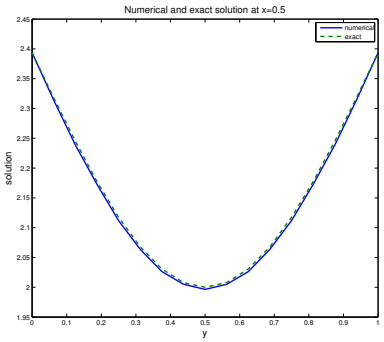

Figure 7. Model 2: Numerical and exact solutions at $x = 0.5$ for v_p.

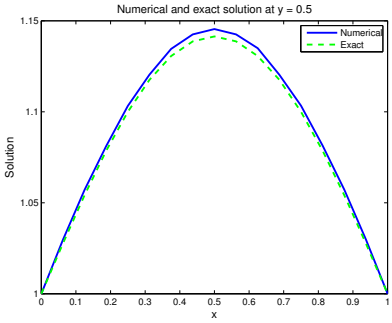

Figure 8. Model 2: Numerical and exact solutions at $y = 0.5$ for v_s.

4.3. Model 3

We assume that

$$v_p = \begin{cases} 3, & \text{for} \quad (x,y) \in [0,0.4] \times [0,1] \\ 3 + 0.8\alpha \int_{0.4}^{x} e^{-\frac{0.01}{(s-0.4)(0.6-s)}}\, ds, & \text{for} \quad (x,y) \in [0.4,0.6] \times [0,1] \\ 3.8, & \text{for} \quad (x,y) \in [0.6,1] \times [0,1] \end{cases}$$

and

$$v_s = \begin{cases} 2, & \text{for} \quad (x,y) \in [0,0.4] \times [0,1] \\ 2 + 0.2\alpha \int_{0.4}^{x} e^{-\frac{0.01}{(s-0.4)(0.6-s)}}\, ds, & \text{for} \quad (x,y) \in [0.4,0.6] \times [0,1] \\ 2.2, & \text{for} \quad (x,y) \in [0.6,1] \times [0,1] \end{cases}.$$

and

$$\rho = \begin{cases} 2.5, & \text{for} \quad (x,y) \in [0,0.4] \times [0,1] \\ 2.5 + 0.5\alpha \int_{0.4}^{x} e^{-\frac{0.01}{(s-0.4)(0.6-s)}}\, ds, & \text{for} \quad (x,y) \in [0.4,0.6] \times [0,1] \\ 3.0, & \text{for} \quad (x,y) \in [0.6,1] \times [0,1] \end{cases}.$$

where

$$\alpha = \frac{1}{\int_{0.4}^{0.6} e^{-\frac{0.01}{(s-0.4)(0.6-s)}}\, ds}.$$

The initial guesses are

$$v_p^{(0)} = 2.5 \quad \text{and} \quad v_s^{(0)} = 1.5$$

and the regularization parameter $\beta = 10^{-4}$. We use $N = 20$ and shoot 20 rays at each source on the boundary.

As for relative numerical errors of the P-wave speed, the relative error initially is 0.2857, and the relative error at the 30-th iteration is 0.0093; thus the relative error is reduced by 30 times in 30 iterations. Similar behavior is observed for the relative errors of the S-wave speed.

In Figure 9, we compare the numerical solution and the exact solution at $y = 0.5$, while in Figure 10, we compare the numerical solution and the exact solution at $y = 0.5$.

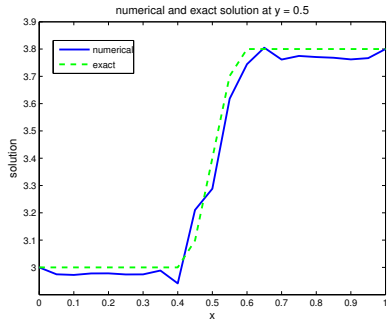

Figure 9. Model 3: Numerical and exact solutions at $y = 0.5$ for v_p.

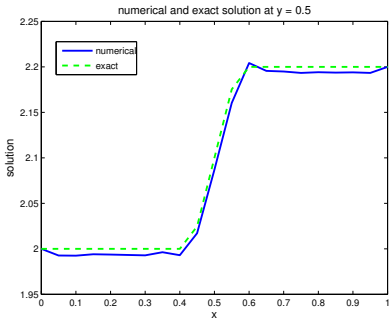

Figure 10. Model 3: Numerical and exact solutions at $y = 0.5$ for v_s.

5. Conclusion

We have developed a phase space method for reconstructing P-wave speed and S-wave speed of an elastic medium from travel time measurements. The method is based on the so-called Stefanov-Uhlmann identity which links two Riemannian metrics in a novel way. Linearizing this identity yields an efficient numerical method for solving the reconstruction problem. In particular, this phase space formulation can deal with multiple arrival times naturally. We have designed numerical algorithms to solve the resulting inverse problem. Numerical examples for elastic-wave traveltime tomography demonstrate the effectiveness of the method.

Acknowledgment

Qian is supported by NSF #0542174, Uhlmann is partially supported by NSF and the Walker Family Endowed Professorship, and Zhao is partially supported by NSF #0513073, ONR Grant #N00014-02-1-0090 and DARPA Grant #N00014-02-1-0603.

References

[1] J. D. Achenbach, A. K. Gautesen, and H. MacMaken. *Ray methods for waves in elastic solids*. Boston, MA: Pitman, 1982.

[2] G. Beylkin. Stability and uniqueness of the solution of the inverse kinematic problem of seismology in higher dimensions. *J. Soviet Math.*, 21:251–254, 1983.

[3] T. N. Bishop, K. P. Bube, R. T. Cutler, R. T. Langan, P. L. Love, J. R. Resnick, R. T. Shuey, D. A. Spindler, and H. W. Wyld. Tomographic determination of velocity and depth in laterally varying media. *Geophysics*, 50:903–923, 1985.

[4] K. P. Bube and R. T. Langan. Hybrid l^1-l^2 minimization with applications to tomography. *Geophysics*, 62:1183–1195, 1997.

[5] E. Chung, J. Qian, G. Uhlmann, and H.K. Zhao. A new phase space method for recovering index of refraction from travel times. *Inverse Problems*, 23:309–329, 2007.

[6] C. Croke, N. S. Dairbekov, and V. A. Sharafutdinov. Local boundary rigidity of a compact Riemannian manifold with curvature bounded above. *Trans. Amer. Math. Soc.*, 352:3937–3956, 2000.

[7] B. Engquist and O. Runborg. Computational high frequency wave propagation. *Acta Numerica*, 12:181–266, 2003.

[8] S. Gray. Efficient traveltime calculations for kirchhoff migration. *Geophysics*, 51:1685–1688, 1986.

[9] M. E. Gurtin. *An Introduction to continuum mechanics*. Academic Press, New York, 1981.

[10] S. Hansen and G. Uhlmann. Propagation of polarization in elastodynamics with residual stress and travel-times. *Math. Ann.*, 326:563–587, 2003.

[11] S. Leung and J. Qian. A transmission tomography problem based on multiple arrivals from paraxial Liouville equations. In *75th Ann. Internat. Mtg., Soc. Expl. Geophys., Expanded Abstracts*, pages 2589–2592. Soc. Expl. Geophys., Tulsa, OK., 2005.

[12] S. Leung and J. Qian. An adjoint state method for three-dimensional transmission traveltime tomography using first-arrivals. *Comm. Math. Sci.*, 4:249–266, 2006.
[13] S. Leung and J. Qian. Transmission traveltime tomography based on paraxial Liouville equations and level set formulations. *Inverse Problems*, 23:799–821, 2007.
[14] Z. Liu and N. Bleistein. Migration velocity analysis: theory and an iterative algorithm. *Geophysics*, 60:142–153, 1995.
[15] J. Locker and P. M. Prenter. Regularization with differential operators. I. general theory. *J. Math. Anal. Appl.*, 74:504–529, 1980.
[16] J. Locker and P. M. Prenter. Regularization with differential operators. II. weak least squares finite element solutions to first kind integral equations. *SIAM J. Numer. Anal.*, 17:247–267, 1980.
[17] R. Michel. Sur la rigidite imposee par la longueur des geodesiques. (French) [on the rigidity imposed by the length of geodesics]. *Invent. Math.*, 65:71–83, 1981.
[18] R. G. Mukhometov. The reconstruction problem of a two-dimensional Riemannian metric, and integral geometry. (Russian). *Dokl. Akad. Nauk SSSR*, 232:32–35, 1977.
[19] R. G. Mukhometov. On a problem of reconstructing Riemannian metrics. *Siberian Math. J.*, 22:420–433, 1982.
[20] M. J. P. Musgrave. *Crystal acoustics*. Holden-Day, 1970.
[21] V. Pereyra. Ray tracing methods for inverse problems. *Inverse Problems*, 16:R1–R35, 2000.
[22] L. Pestov and G. Uhlmann. Two dimensional compact simple Riemannian manifolds are boundary distance rigid. *Ann. Math.*, 161:1093–1110, 2005.
[23] J. Qian, L.-T. Cheng, and S. J. Osher. A level set based Eulerian approach for anisotropic wave propagations. *Wave Motion*, 37:365–379, 2003.
[24] J. Qian and W. W. Symes. Paraxial eikonal solvers for anisotropic quasi-P traveltimes. *J. Comput. Phys.*, 173:1–23, 2001.
[25] J. Qian and W. W. Symes. Finite-difference quasi-P traveltimes for anisotropic media. *Geophysics*, 67:147–155, 2002.
[26] V. G. Romanov. *Inverse problems of mathematical physics*. VNU Science Press BV, Utrecht, The Netherlands, 1987.
[27] A. Sei and W. W. Symes. Gradient calculation of the traveltime cost function without ray tracing. In *65th Ann. Internat. Mtg., Soc. Expl. Geophys., Expanded Abstracts*, pages 1351–1354. Soc. Expl. Geophys., Tulsa, OK, 1994.
[28] A. Sei and W. W. Symes. Convergent finite-difference traveltime gradient for tomography. In *66th Ann. Internat. Mtg., Soc. Expl. Geophys., Expanded Abstracts*, pages 1258–1261. Soc. Expl. Geophys., Tulsa, OK, 1995.
[29] V. A. Sharafutdinov. *Integral geometry of tensor fields*. VSP BV, Utrchet, The Netherlands, 1994.
[30] P. Stefanov and G. Uhlmann. Rigidity for metrics with the same lengths of geodesics. *Math. Res. Lett.*, 5:83–96, 1998.
[31] P. Stefanov and G. Uhlmann. Boundary rigidity and stability for generic simple metrics. *J. Amer. Math. Soc.*, 18:975–1003, 2005.
[32] P. Stefanov and G. Uhlmann. Boundary and lens rigidity, tensor tomography and analytic microlocal analysis. *submitted*, 2006.
[33] M. E. Taylor. *Partial differential equations: basic theory*. Springer-Verlag New York, USA, 1996.
[34] J-N Wang. Stability for the reconstruction of a Riemannian metric by boundary measurements. *Inverse Problems*, 15:1177–1192, 1999.
[35] J. K. Washbourne, J. W. Rector, and K. P. Bube. Crosswell traveltime tomography in three dimensions. *Geophysics*, 67:853–871, 2002.